Nanomechanical behaviour of Polystyrene/Graphene Oxide nanocomposites

Zaid G. Mohammadsalih [a, b, *], Nic Mullin [c], Sergiu Amarie [d], Artem Danilov [d], and Ihtesham Ur Rehman [e]

[a] Applied Science Research Unit, Applied Science Department, University of Technology– Iraq.

[b] Advanced Engineering Materials and Composites Research Centre (AEMC), Department of Mechanical and Manufacturing Engineering, Universiti Putra Malaysia, 43400 UPM Serdang, Selangor, Malaysia.

[c] Department of Physics and Astronomy, University of Sheffield, Sheffield, S3 7RH, UK.

[d] Attocube Systems, Munich, Germany.

[e] School of Medicine, University of Central Lancashire, Preston, Lancashire PR1 2HE[*]Corresponding author Email Address: Zaid.G.Mohammadsalih@uotechnology.edu.iq

Address: Street No. 52, Karrada, P.O. Box: 19006, Baghdad, Iraq.

Abstract

The In-situ investigation for the nanomechanical features of the polymer graphene nanocomposites has become a challenging and an indispensable task to achieve the required application. Graphene oxide (GO) nanocomposites were prepared at 1.0% weight fraction of GO to reinforce polystyrene (PS) using solution blending approach. The morphology of the resulting nanocomposites was characterized by optical, scanning electron, transmission electron, atomic force and scattering scanning near-field optical microscopies. These showed a uniform dispersion of graphene oxide nano-sheets in the PS matrix. By adopting Derjaguin Muller Toporov (DMT) formula, the nanomechanical properties for the cryogenically fractured surface of the composites were characterized using the traditional Atomic Force Microscopy (AFM), Peak-Force Quantitative Nanomechanical Mapping (QNM), and Tip-Force mode functioned with scattering scanning near–field optical microscopy (s-SNOM). Young's modulus of the PS matrix varied around (1-2) GPa as shown by QNM and s-SNOM similar to what was reported in the literature. However, while putative GO nano-sheets were measured to have a higher elastic modulus than the surrounding matrix in Peak-Force QNM experiments, they were significantly below literature values. By using Tip-Force mode related to s-SNOM, the expected values of Young's modulus for GO were recovered.

Keywords: Polystyrene, Graphene Oxide, Young's Modulus, Nanomechanics, Derjaguin Muller Toporov.

Introduction

In nano-scale regime, the materials are exhibiting a considerably different mechanical features compared to their counterparts in macro-scale system.

The carbon based nano fillers have drawn a serious attention due to their unique features such as low cost, low weight and ease of processing [1]. Graphite, fullerene, carbon nano tubes and the recently discovered material, graphene, are derived from this fascinating material, carbon. These are the most studied allotropes by the technologists and researchers [2]. Graphene is a planar honeycomb lattice that has a two dimensional and one atom thick carbon sheet with a molecular bond length of 0.142 nm. High thermal conductivity, high intrinsic mobility, optical transmittance of 98%, large specific surface area, and high Young's modulus are the most important outstanding physical properties for a single sheet of defect free graphene [3].

These properties have participated effectively to broaden the horizon towards different applications in many disciplines such as sensors, energy conversion, storage devices, solar cells and reinforced composites [4].

To ensure an ideal exploitation for these unique properties in numerous kinds of applications, graphene and its derivatives have been successfully prepared using versatile routes of preparation such as top down exfoliation of graphite by means of oxidation, to the bottom-up chemical vapour deposition [5].

Graphene cannot be directly employed to reinforce polymers as a result of high π-π interaction, GO is usually incorporated into polymer matrices for making high quality polymer nanocomposites (PNCs).

GO has better compatibility with polymers, uniform dispersion can be obtained via mixing it with different polymer matrices using different strategies, and it provides a possibility of mass production [6].

The structure of GO may be considered as a graphene sheet associated with an abundance of oxygenated functional groups represented by hydroxyl and carboxyl functional groups at the peripheries, carbonyl and Epoxy functional groups at the basal plane [7, 8]. PS is one of the most common and widely used thermoplastics. It can be used in many kinds of applications such as construction, automotive, and protective packaging [9]. The combination of nano-fillers that have at least one dimension in the nanoscale (1-100) nm and the polymer matrix are known as nanocomposites which have a wide range of applications represented by, but not limited to, automobiles, sport products, and aerospace [10, 11]. There has been a rapid growth of interest in nanomechanics in recent years with the emergence of nano-scale materials, mechanics based applications of such materials and novel mechanics phenomena at the nano-scale [12].

AFM based force spectroscopies, in which force vs. distance curves are collected, converted into force vs indentation curves and analyzed using appropriate contact mechanics models, allow mechanical properties including stiffness, adhesion and Young's modulus to be mapped with nanoscale resolution.

This measurement technique also enables imaging of the topography of solid surfaces at high resolution [13]. Since its invention in 1986, AFM has become an indispensable tool for investigating the nanomechanical behaviour of polymer matrices and nano-particles through its capability for imaging surfaces at very high resolution and measuring different short-range forces near the surface of a material.

With regard to the force measurements, depending on the situation different forces including Van Der Waals, capillary forces, chemical bonding, electrostatic forces and magnetic forces can be characterized of distance to the AFM tip [14].

DMT model is useful for analysis using low loads in which the surface forces become important. There are limitations for this theory however and the most important is the assumption of Hertzian deformation only. This assumption can lead to an underestimation of the contact area, but it is still within reasonable limits to justify its use. The theory of DMT is more applicable to systems that have low work of adhesion and high elastic moduli [15]. Given the aforementioned assumption the DMT modulus can be calculated from the following equation:

$F_{tip} = 4/3\ E^* (Rd^3)^{1/2} + F_{adh}$ ……………………….. (1)

Where F_{tip} is the applied force on the tip, R is the radius of the tip, d is the deformation of the sample, F_{adh} is the force of adhesion and E* is the reduced modulus [16]. In 2012, a couple of researchers were measured the elastic modulus of three kinds of polymers, PS was among them, using AFM with employing of steel micro- spherical probe tip. The used models for finding the moduli was Hertz and Johnson-Kindall-Roberts (JKR). The indentation depth was 1.7 nm and the elastic modulus for the PS was 2.6 GPa [17]. The rectangular shape or ‘’Diving board’’ and ‘’V’’ shape cantilever are the main two shapers of cantilevers both of which are mainly micro-fabricated from silicon or silicon nitride. The V shape cantilevers are the most popular and widely used cantilevers due to their high lateral stiffness [18].

In recent years, a new mode of AFM, known as Peak Force Tapping (PFT), which operates using a sinusoidal tapping motion at frequencies significantly below the resonant frequency of the cantilever, and utilizes the deflection signal (force) at the position of closest approach for topographic feedback has become popular.

A key advantage of this technique is that it allows force vs. distance curves to be acquired at much higher frequencies than conventional force-volume imaging, allowing high resolution force maps to be captured in minutes as opposed to hours. An extension to PFT, known as QNM allows real-time processing of the force-distance curves to simultaneously produce maps of Young's modulus using the DMT model for the tip-sample contact.

Young's modulus at nano-scale for polypropylene (PP) nano-silica nanocomposites that contain styrene-(ethylene-co-butylene)-styrene (SEBS) using QNM has been reported before, where the collaborators used the DMT model with a silicon tip that has a nominal radius of 8 nm and the modulus for the PP nano-silica nanocomposites had the highest value compared with PP nanocomposites that contain SEBS [19].

In another study, same technique of peak force QNM and the DMT model, for measuring the Young's moduli for a number of polymers using a range of probes. They used three kinds of probes manufactured from different materials with different spring constants, and compared them with the results obtained by nano-indentation. Polymethyl methacrylate (PMMA) was found to have the highest value of Young's modulus [20]. Dealing with complex morphologies represents a key challenge in the field of PNCs, as it is important to identify filler particles from the surrounding polymer matrix.

High chemical sensitivity and high spatial resolution of the emerging infrared nano-spectroscopy combined with atomic force microscopy AFM-IR, photo-induced force microscopy PIFM, and scattering type scanning near field optical microscopy s-SNOM are the useful tolls that can be used to for the characterization of nanocomposites [21]. S-SNOM provides good spatial resolution. Currently, this technique possesses good lateral optical resolution whilst the infrared IR, the combined tool with s-SNOM, is capable of recognizing the chemical specificity down to 5.0 nm with a 100 nm spatial optical resolution. It is considerably powerful analytical technique due to its uniqueness in combining the high chemical specificity of IR with the high spatial resolution associated with s-SNOM allowing to obtain both physical and chemical information from surface of the nanocomposites. It is useful for analyzing organic matter as it provides high accuracy and precision for such materials [22, 23]. Beside the ability of exploring the nanomechanical behaviour for polymer nanocomposites, s-SNOM can be utilized in applications such as imaging electrical and magnetic near fields, surface Plasmon imaging, infrared nano imaging, organic bulk heterojunction (BHJ) solar cells, and improve the design and performance of optoelectronic devices [24]. The work described in this paper investigated the nanomechanical behaviour of GO nano-sheets in combination with PS acting as the host material. Low weight fraction of 1.0wt. % was employed to reinforce PS. The cryogenically fractured surface was investigated to image the nano-sheets of GO as well as evaluating Young's modulus at nano-scale. The preparation of graphite oxide, GO, PS and nanocomposite have been studied and published previously [25, 26], where the optimum conditions of preparation confirmed. The novelty of this work is represented by managing the unprecedented challenge of performing range of sophisticated microscopic investigations in order to evaluate the nanomechanical

behaviour of the polymer and the included nano-additive for a cryogenically fractured surface of ~ 1.0 mm of thickness. The majority of work in this filed was carried out for the flat surfaces of different kinds of polymer nanocomposites. It is most unlikely to perform nanomechanical experiments in such profound conditions.

Experimental Procedures

Materials

Beads of PS were obtained from Dow chemicals (Styron 634, Dow Chemical Company, obtained from RESINEX, UK). The grain size of the graphite powder used to prepare graphite oxide was ≤ 20μm. Other chemicals used in this study and their specifications are; sulphuric acid (95- 98 %), potassium permanganate (97%), sodium nitrate (>99%), hydrochloric acid (36.5%) in water, hydrogen peroxide (29 – 32) % in water, and Tetrahydrofuran THF (>99.5%). All of the aforementioned chemicals were obtained from Sigma Aldrich.

Preparation of graphite oxide, graphene oxide and nanocomposites of PS/GO

Graphite oxide was prepared according to the procedure described previously by a research group [27]. Graphite 6.0 g was mixed with 3.0 g of $NaNO_3$ in a beaker. Concentrated H_2SO_4 (138 ml) was added to a beaker which was placed in an ice bath to keep the reaction temperature below 35 $^{\circ}$C. Then, 36 g of $KMNO_4$ was added slowly, gradually, and cautiously over 48 hours while maintaining stirring. A yellow brown viscous mixture was obtained. To reduce the viscosity of the reaction mixture, (10-15) ml of H_2O_2 was added. Graphite oxide was washed with dilute HCl-distilled water until the pH reached ~ 6.0. Obtained solution was centrifuged at 8000 rpm for 1.0 hour.

A specific procedure was followed to prepare GO which was clarified in a previous work [26, 28]. Graphite oxide was sonicated for 1.0 h and centrifuged for 0.5 hour at 6000 rpm. The suspension was casted in metallic dishes and left to be frozen in a freezer for 48 h at -50 ºC followed by freeze drying (lyophilization) for 72 hours under vacuum of 10^{-1} bar. Finally, GO was obtained as a flossy powder.

Nanocomposite was prepared in THF. PS pellets 20 g were fully dissolved in 200 ml of THF while maintaining stirring for 2.0 h. GO 300mg was added in 300 ml of THF and stirred for 2.0 h and sonicated for 30 min. GO/THF suspension was added to PS/THF solution while maintaining stirring. The weight fractions for GO in PS/GO nanocomposites was 1.0 wt. %, and the mixed solution was stirred for 1:30 h, followed by sonication for 1.0 h and 1.0 h of shear mixing at 1600rpm /Amp 0.3.

The obtained suspension of PS/GO was poured in glass covered Petri-dishes to ensure a slower evaporation of the solvent. All samples were left in fume cupboard for a week and then in vacuum oven for 3.0 hours and 50°C to be fully dried. A cryogenic fracture surface was obtained via snapping the nanocomposite sample in liquid nitrogen. The sample was soaked in a container of liquid nitrogen for five minutes and it was snapped inside the container for obtaining a clean fracture surface.
Figure 1 shows the cryogenically fractured surface of the PS/GO 1.0 wt. %. Then, it was fitted over a sample holder. The thickness of the measured cryogenic fractured surface was ~ 1.0 mm. The nanomechanical measurements in different microscopic tools were carried out for that cryogenically fractured surface as it was so difficult to find the nano-sheets of GO via the bulk polymeric surface due to the low weight fraction employed in the current study.

Figure 1: The cryogenically fractured surface of the nanocomposite of PS/GO 1.0 wt. %.

Characterization

Fourier Transform Infrared Spectrometry

Fourier Transform Infrared Spectrometer (FTIR Spectrum 100™ Perkin Elmer, USA) was used to obtain spectra within the mid-IR range of 4000-400 cm^{-1} of graphite oxide, GO, PS and PS/GO nanocomposite. Spectra were obtained by accumulating 16 number of scans at 4.0 cm^{-1} resolution.

Scanning Electron Microscopy

Scanning electron microscopy (SEM Inspect F™), Poland; was used to characterize GO and the fracture surface at 10 kV. Nanocomposite sample was coated manually with silver dag followed by gold coating for 3.0 minutes using a sputter coater machine (Emscope SC 500™, England), whereas GO coated by gold only as there was no need to use the silver dag to coat the GO fluffy powder.

Optical Microscopy

The optical microscopy (OM) made by (Swift, New York Microscope Co. USA) was used for imaging the nanocomposites at 10X magnification to confirm an outset indication about the distribution of GO in PS matrix.

Transmission Electron Microscopy

For investigation the quality of dispersion of the nano-sheets in the matrix, transmission electron microscopy (TEM) was used. Sample of PS/GO 1.0 wt. % was

snapped frozen in Liquid Nitrogen and placed in the FC6 cryo chamber to equilibrate for 30 minutes. Ultrathin sections, approximately 90-100nm thick, were cut using an ultra-microtome and FC6 cryo-box attachment onto uncoated 200 mesh copper grids at temperatures of between -60 to -100 °C. Sections were examined using a FEI Tecnai™ TEM at an accelerating voltage of 80Kv and 100Kv. Electron micrographs were obtained using a Gatan Orius 1000™ digital camera and Gatan digital micrograph® software.

AFM

Young's modulus of the GO/PS nanocomposite was obtained by applying the DMT approach for the aforementioned cryogenically fractured surface. A silicon nitride based cantilever was used to analyze fractured surfaces of the nanocomposites.

The length of the cantilever was 200 μm, the spring constant was 0.08 Nm^{-1}, the resonance frequency was 17 KHz and the tip radius was 5 nm. Mechanical properties at the nanoscale for the same cryogenically fractured surface were obtained via peak force QNM using a Dimension Icon AFM (Bruker), USA. Deflection sensitivity was found for the cantilever (TESPA-V2) after making 10 indentations over a surface of Sapphire and the average for them was considered as the average deflection sensitivity which was 67.9 $nm.V^{-1}$. Thermal noise method (an analysis of the power spectral density of displacement fluctuations of the cantilever in contact with a thermal bath) was performed for finding the stiffness of the cantilever which was 45.6Nm^{-1}. The tip radius was estimated using the relative calibration method, in which a scan of a PS/LDPE blend was taken and the estimated tip radius was iterated until the expected modulus matched the measured value. This process yielded a tip

radius of 17 nm. The PeakForce amplitude was 10 nm, the tapping frequency was 1.0 kHz and the PeakForce set-point was 10 nN.

Before any nanomechanical measurements were made, the sample was scanned in Tapping Mode (using the same probe) in order to locate regions of interest. The cantilever was tuned to a free amplitude of approximately 15 nm and the amplitude set-point was approx. 12 nm. Scans were acquired at a line rate of 0.5-1 Hz. Gwyddion™ software was used to manually draw a mask over putative GO flakes in the DMT modulus channels. Mean and standard deviations for the measured Young's modulus were measured for histograms of the flake and matrix regions.

To obtain a complementary conclusion about the nanomechanical behaviour for the PS/GO nanocomposites, s-SNOM tool was employed obtain Young's modulus for the soft material represented by the polymer as well as the rigid inclusions that reinforced it represented by GO nano-sheets. This also allowed to obtain mechanical, thermal, optical, and electrical properties at nano-scale. The mechanical noise was below 0.2 nm with a fixed tip position. The integrated bright field microscope was used with an apochromatic objective and field of view was adjusted to be 700 µm. A motorized positioner was employed to obtain a precise focusing. The positioning accuracy was less than 10 nm. The scan range was specified to be (100 *100) µm. A laser source of wavelength of 633 nm was coupled with the near field microscope.

Results and Discussion

FTIR

Figure 2 shows the IR spectra for the different materials present in the fabricated nanocomposite.

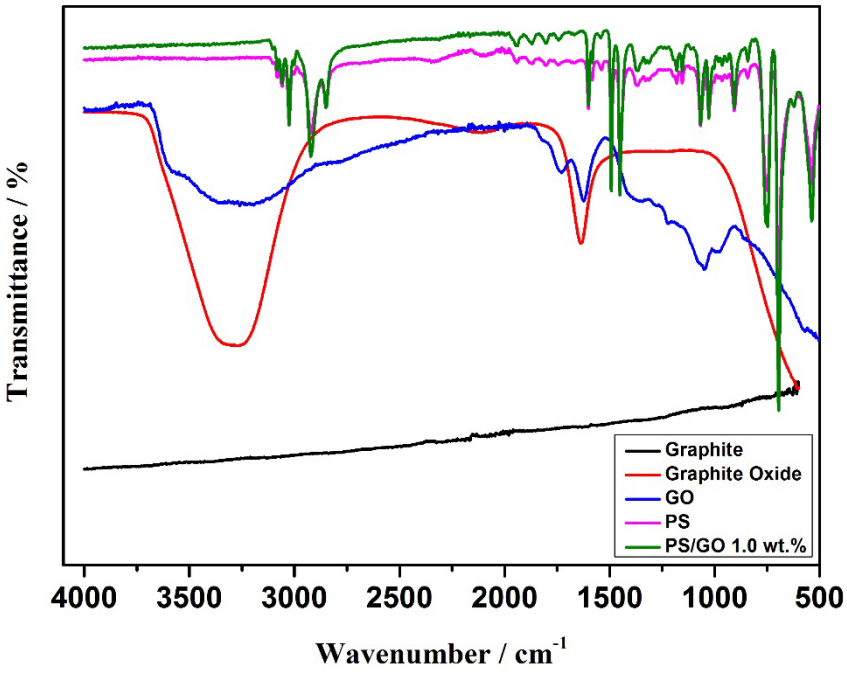

Figure 2: IR spectra for graphite, graphite oxide, GO, PS, and PS/GO of 1.0 wt. %.

Pure graphite is not exhibited any considerable absorption band at the studied region of IR spectroscopy which reflected its chemical inertness [29, 30]. The effect of oxidation process can be seen in the spectra of graphite oxide and GO, respectively. For the graphite oxide spectra, two main peaks can be found, the first one is the most prominent one located at 3286 cm^{-1} attributed to the C-OH stretching vibrations of the hydroxyl group. The other peak that can be seen for the graphite oxide is present at 1620 cm^{-1} due to C=C skeletal vibration of the non-oxidized graphite [31].

Presence of a broad peak located between (3700 – 3000) cm^{-1} attributed to free and adsorbed hydroxyl functional groups has also been reported in literature.

In addition, a peak centered at 1620 cm^{-1} ascribed to the deformation vibration of adsorbed water molecules has also been reported [30]. The GO spectrum shows an

abundance of oxygenated functional groups represented by carboxylic acid groups, epoxide and hydroxyl. The broad peak located around 3500 cm^{-1} refers to the stretching vibration of O-H. The other absorption peaks of C = O from the absorption of carbonyl and carboxylic acid groups, C = C from the unoxidized graphitic domain, C – H and C – O from the absorption of epoxy groups can be seen at (1720, 1450, 1340 and 1100) cm^{-1} wavenumbers; respectively. All of the vibrations are stretching vibrations apart from the C – H group which has a bending vibration [26, 32]. For the spectrum of PS, The aromatic stretching vibration of =C-H can be seen within the range of (3100-3000) cm^{-1}. The peaks located at 2929 cm^{-1} and 2849 cm^{-1} refer to asymmetric and symmetric stretching; respectively. These are associated with the vibration of CH_2. The stretching vibration of benzene ring are linked with the peaks located at (1600, 1580, and 1491) cm^{-1}. The C-H out of plane bending vibration of the benzene ring can be seen at 753 and 697 cm^{-1}. The spectrum related to PS/GO 1.0 wt. % is similar to the abovementioned one related to PS. The overlap between GO and PS peaks makes the detection of a typical peak of interaction between the two materials quite difficult. Probably, there is a weak peak that refers to a possible interaction between PS and GO located at 1073 cm^{-1}. The type of interaction is most likely to be π-π stacking. Table 1 summarizes the findings of IR spectra.

Table 1: IR spectra findings for graphite oxide, GO, PS, and the nanocomposite of PS/GO 1.0 wt. %.

Material	**Functional group**	**Wavenumber /cm^{-1}**
Graphite Oxide	C-OH	3286
	C=C	1620

GO	O-H C=O C=C C-H C-O	3500 1720 1450 1340 1100
PS	=C-H Asymmetric CH_2 Symmetric CH_2 Benzene ring, stretching C-H out of plane Benzene ring, bending	3100-3000 2929 2849 1600, 1580, 1491 753, 697
PS/GO	* Same functional groups of PS * Possible π-π interaction of PS and GO	1073

SEM, TEM, and OM findings

Figure 3 shows micrograph of the fracture surface of the neat polymer and the nanocomposite.

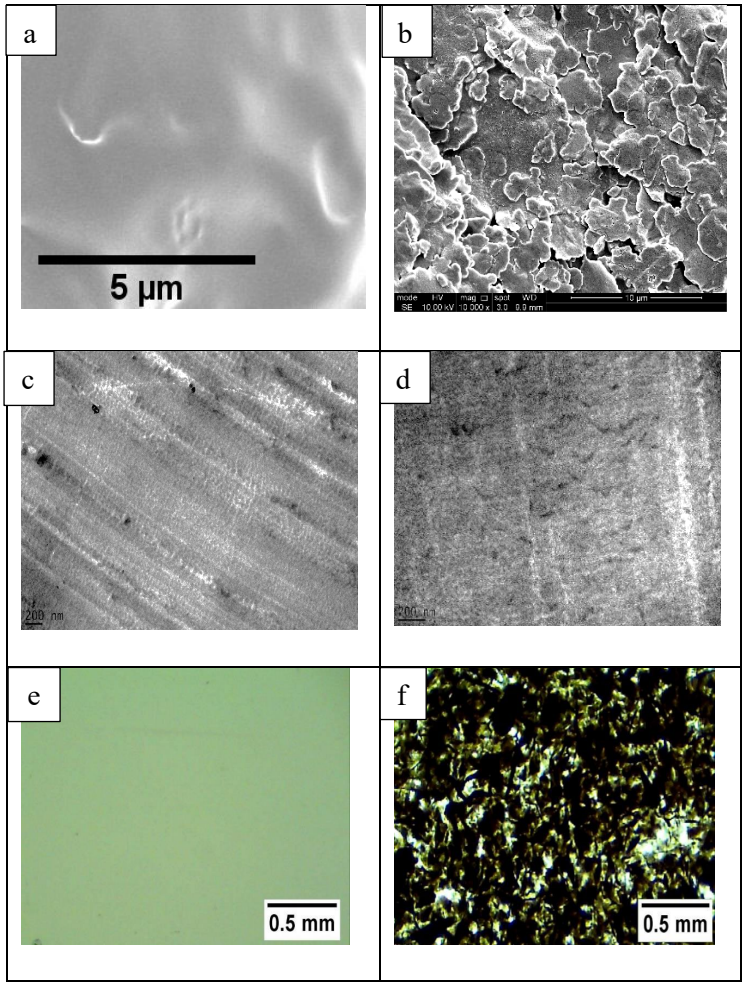

Figure 3: (a-b) SEM images for the fracture surface of PS and PS/GO 1.0 wt. %, respectively. (c-d) TEM images for the fracture surface of PS and PS/GO 1.0 wt. %, respectively. (e-f) Optical Microscopy images for different cross - sections of PS and PS/GO 1.0 wt. %; respectively.

Figure 3 a shows the smoothness and uniformity of the cryogenically fractured surface of the neat polymer compared with the rough fracture surface of the nanocomposite sample of PS/GO 1.0 wt. % which is shown in Figure 3 b both are achieved by SEM. The incorporation of GO flakes for reinforcing purposes is the main reason behind the roughness of the cryogenically fractured surface compared to the neat polymer. Aggregates of GO in a few random places can be seen in the morphology of the lower couple of images for the nanocomposites. However, good dispersion of GO flakes in PS can be seen according to the employment of synergistic techniques of dispersion.

Similar findings have been reported in 2013 [33], where a few stacks of 1.0 wt. % of graphene was incorporated in the PS matrix, as the concentration of graphene was increased, higher amount of agglomerations obtained. They also referred to the uniform morphology of the PS, and the somewhat decreased roughness for the nanocomposites as they included 1.0 % weight fractions of graphene nano-powder. All the findings for the matrix and nanocomposites were obtained via the cryogenically fractured surfaces. In another study, distribution of graphene nanoplatelets in polyurethane PU has been reported where agglomeration of the nanoplatelets in the polymer was observed as they incorporated 2.0 wt. % of the aforementioned nanomaterials as a reinforcement agent [34]. Figure 3 (c & d) shows the TEM images of PS and PS/GO 1.0 wt. %, respectively. The black sheets represent the nano-sheets and the grey background represents the polymer. In order to show the difference in morphology between the neat polymer and the nanocomposite, a featureless image for pristine PS is recorded. In the 2nd image that shows the nanocomposite, curved and partially peeled nano-sheets can be seen which provide an impression of the morphology of the nanocomposite material. Aggregations and stacking for the nano-sheets of GO cannot be found in the PS matrix. These results are in line with the findings reported previously in 2012 [35]. Figure 3 (e and f) refers to the cross sections of the neat polymer matrix of PS, and the relative even distribution of GO in the polymer matrix; respectively. Both images are obtained by utilizing OM. No recognizable objects are found for the pure PS as shown in Figure 3 e which is in line with the findings discussed previously (Figure 3, a and c) obtained by SEM and TEM; respectively.

Figure 3 f is elucidating the homogeneous distribution of GO nano-sheets in the pure PS which is in line with the findings discussed previously (Figure 3 b and d) captured by SEM and TEM; respectively. The best properties of the nanocomposites are only

achievable with a uniform distribution for the nano-fillers in different polymer matrices. The performance of the nanocomposite material is negatively affected as the nano-scale reinforcements tend to coalesce into macro size agglomerates [36]. Previous studies reported in literature confirmed the employment of OM to investigate the distribution of nanomaterials within some polymer matrices [37].

AFM

In order to estimate the Young's modulus of PS and GO nano-sheet at the nano-scale, force-distance curves were measured using AFM with a cantilever that had a very low spring constant. The Young's modulus was calculated from the data using the DMT mathematical formula [38, 39].

Figure 4 (a) and (b) shows the measured force – distance curves for PS and the GO in the nanocomposite respectively along with AFM images for each measured material. These curves and images were taken for the cryogenic fracture surface. Both force-curves for the polymer and the nano-sheet show a saw tooth shape in the region of the pull-off force but it is much more prominent for the GO compared with PS. This means that no artefacts were observed during the pull-off force measurements [40]. It has been reported [41] that the adhesion forces for different kinds of tips and different polymer surface including PS is within the range (- 1.5 nN to -8 nN). It is estimated that the adhesion force for the PS force-distance curve is about -10 nN.

The mounting of fracture surface to the cantilever's tip was a challenge as the thickness of the surface is quite low and as a result detecting this surface topography was not easy to perform.

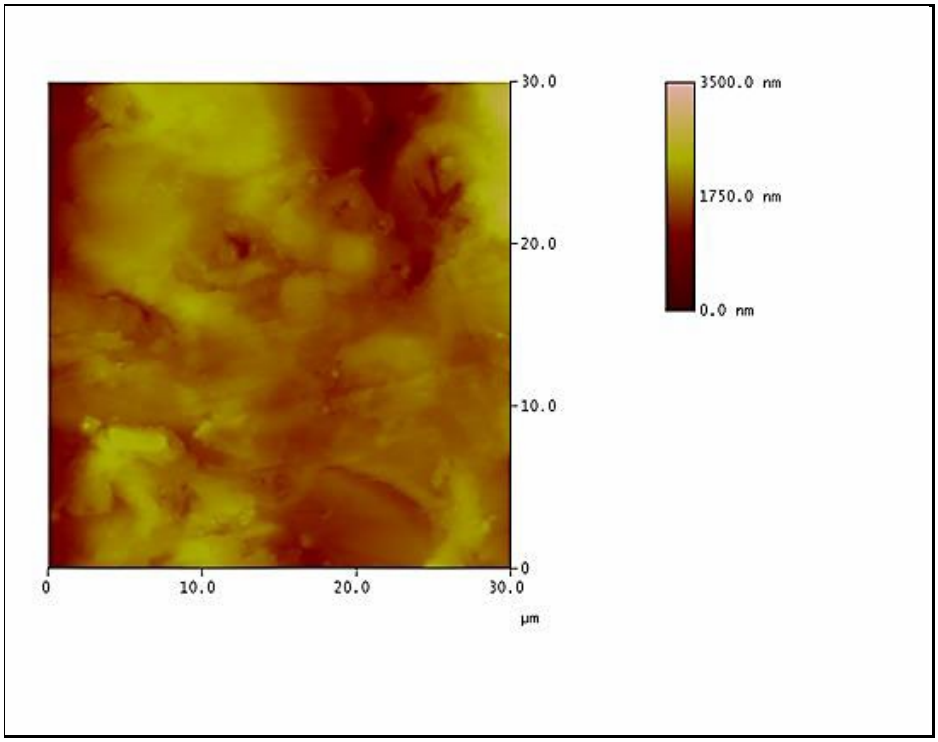

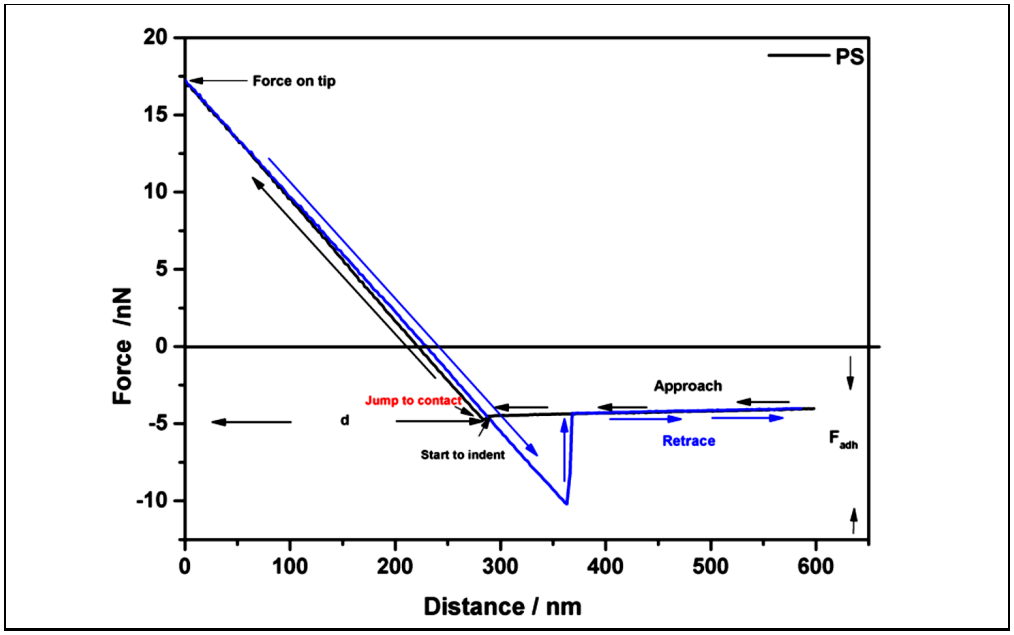

Figure 4 (a): Force-Distance Curve for PS with AFM image for the area where the tip was indented.

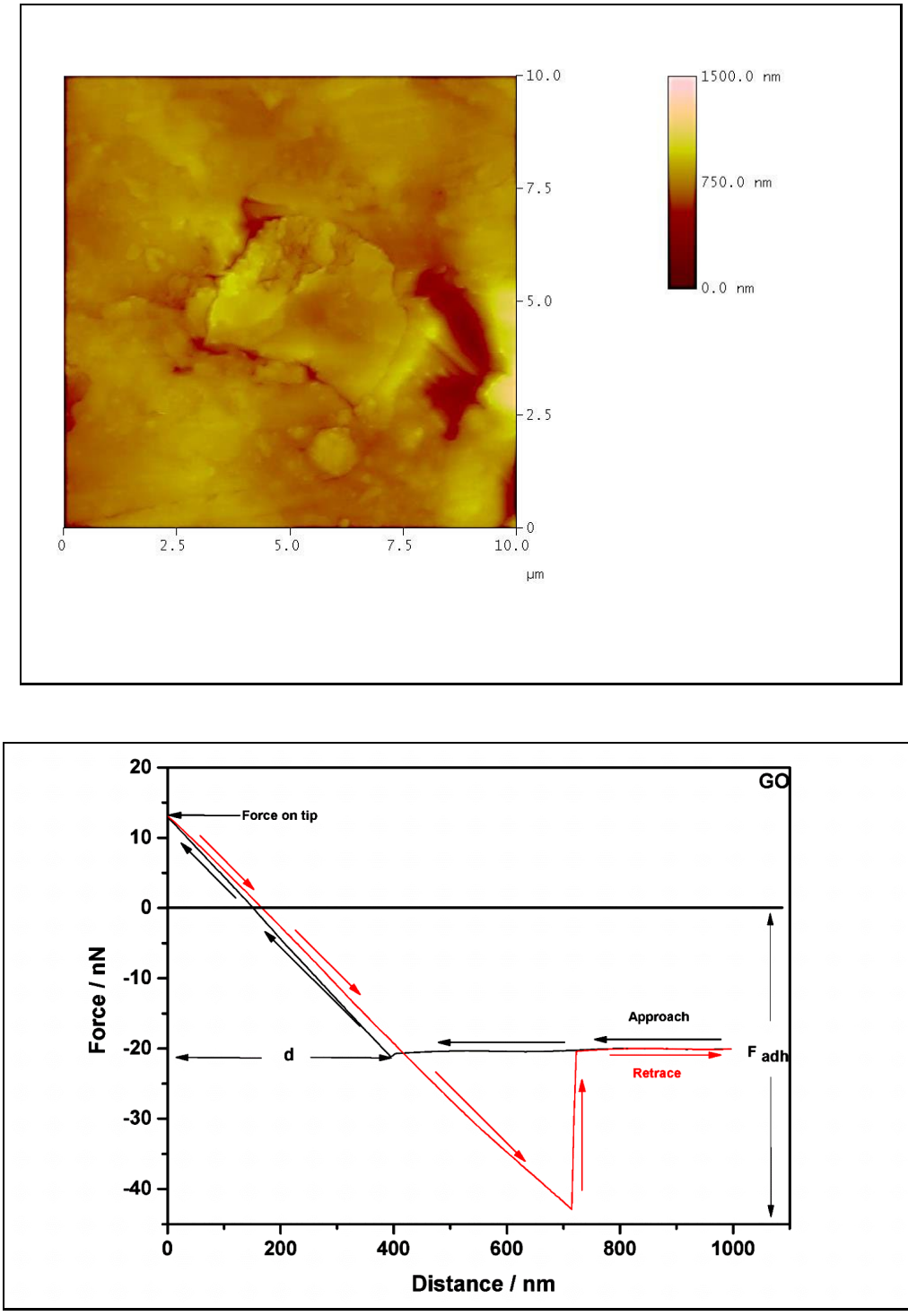

Figure 4 (b): Force-Distance curve for GO nano-sheet with AFM image where the tip was indented.

The procedure for obtaining the force – distance curves begins by adjusting the tip so that it initially stands away from the studied fracture surface. Gradually, it is brought towards the cryogenic fracture surface.

The tiny deflection in the curve indicates that the forces of attraction near the surface pull the tip down when it is in very close proximity with the surface. The tip is then traversed across the surface and deflected by varying degrees by the surface features. When the tip retracted from the studied surface, it ascends until the forces are in equilibrium with other surface forces and the cantilever relaxes downwards. As the probe is lifted from the surface, the cantilever bends downward as the attraction forces hold onto the cantilever, and finally it breaks free with a sharp rebound upwards. The remainder of the force curve shows the operation of the tip leaving the surface back to its original position [42]. Many of the data obtained from adhesion force test were scattered widely with poor reproducibility. Some of the more important sources of error in these measurements leading to a poor evaluation for the adhesion force are: 1- The wrong consideration for the surface roughness. 2- The varying deformation of the tip and the surface. 3- The adsorption of contaminants for both the tip and surface [41]. The cantilever is made from Si3N4 with 200 μm length and spring constant of 0.08 Nm^{-1} (details provided by the manufacturer). One of the aim in this study was to understand nano-mechanical behaviour for the PS and GO before carrying out the QNM and s-SNOM measurements. The thickness of the cryogenic fracture surface was about 1.0 mm.

It is important to emphasize that the main reasons for the selection of this surface rather that the wide flat surface of the sample is that the reduction of the contact area (which is originally obtained cryogenically) plays a dominant role in the reduction of surface roughness and in the reduction of any possible contamination. Moreover, the selected cantilever has a very low spring constant in order to obtain high sensitivity.

If the cantilever is much softer than the tip-sample stiffness (as is the case here), there is a large deflection in the cantilever which consequently affect the reality of indentation, and the measurement is dominated by the uncertainty in the deflection sensitivity of the AFM. It is likely that this is the cause of the very low modulus values for both the PS and GO. Another consideration is thickness, as the length of the cantilever plays an important role in obtaining a large deflection at small force. Rectangular shaped cantilever was selected for this test to ensure high lateral stiffness. The data for the force distance curves are the results of two contributions, the elastic force of the cantilever, and the tip – sample interaction [14]. According to the DMT model, Young's modulus is calculated via unloading part of the force-distance curve. The DMT is a modified Hertzian model that takes into account the force of adhesion between the tip and surface of the sample [20]. The force-curves show clear contact point, repulsive range in the approaching part, and a pull-off point in the retracing part. The Young's modulus for PS was recorded at 2.66 MPa and 8.93 MPa for the GO flake shown in AFM image. Young's modulus at the nano-scale for PS and GO was much higher than these values. The maximum applied load in these experiments was not sufficient to obtain values that were similar to theoretical values or what has been reported in literature [41].

QNM

Peak force QNM has the capability for determining the local mechanical properties at nano-scale resolution unlike the conventional AFM used to characterize the structure and morphology [19]. Measurements were carried out at ambient temperature.

The obtained images shown in Figure 5 have a resolution of (256x256) pixels and scanning rate of 0.528 HZ for the upper left GO flake and (512x512) pixels with a scanning rate of 0.476 HZ for the lower right GO flake. Scanning size started from (30*30) μm^2 and it went significantly down to (1.5*1.5) μm^2 with the detection of GO flakes.

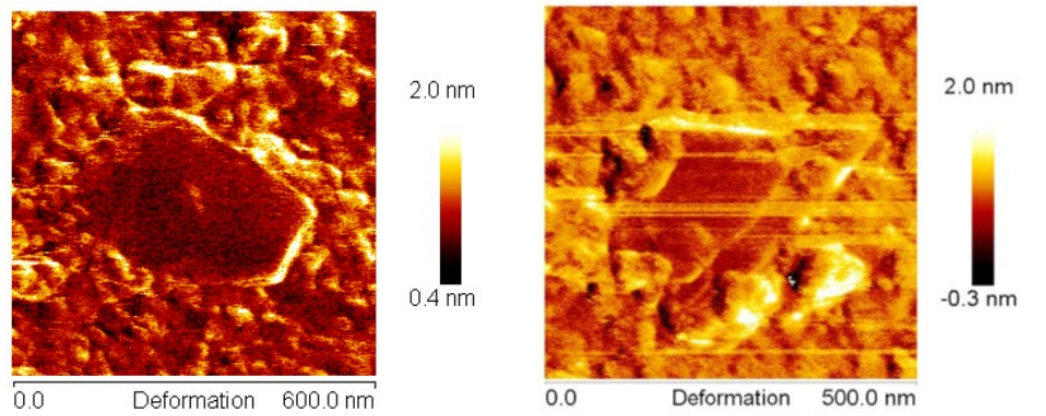

Figure 5: The deformation of upper left and lower right GO flake.

Quantitative measurements for Young's modulus can be carried out by performing a force-distance curve at every pixel in the image and using the peak force as a feedback. Nanoscope™ software was utilized for finding the modulus using the DMT model [43]. Figure 6 –a represents 30 microns morphological characterization of the height sensor channel showing the general topography of the cryogenic fracture surface. A randomly selected area shown with an arrow in the same image is specified for looking to nano-fillers where two recognizable GO nano-sheets were found using the tapping mode. This tapping mode characterization has paved the way towards finding the modulus for PS and GO nano-sheets using the DMT approach.

These measurements provided insightful and comprehensive details of the nanoscopic morphology for the nanocomposites and was deployed as a mapping technique for the nanocomposites before exploring the local nanomechanical properties [19].
Figure 6 b shows the topography of the area indicated by the orange arrow in Figure (a) and this topography is shown by the height sensor channel.

The light diagonal feature across this image -b- shows two flakes. These are in the upper left and the lower right of the light diagonal area.

It should be noted that finding two flakes in a randomly selected area in the cryogenic fracture surface gives an indication of the even distribution of GO flakes in the polymer matrix. The size of these flakes can be estimated as the height differences shown in image –c- does not have any effect on these topographic maps [44].

Due to the large roughness of the freeze-fractured surface, it is difficult to see the GO sheets in the height sensor images of Figure 6 a and 6 b. Image –c- represents the phase channel of the previous image, which shows much clearer contrast between the GO sheets and the PS matrix. The contrast in this channel is related to the energy dissipation from the cantilever. In other words it is related to material properties of the tip sample contact.

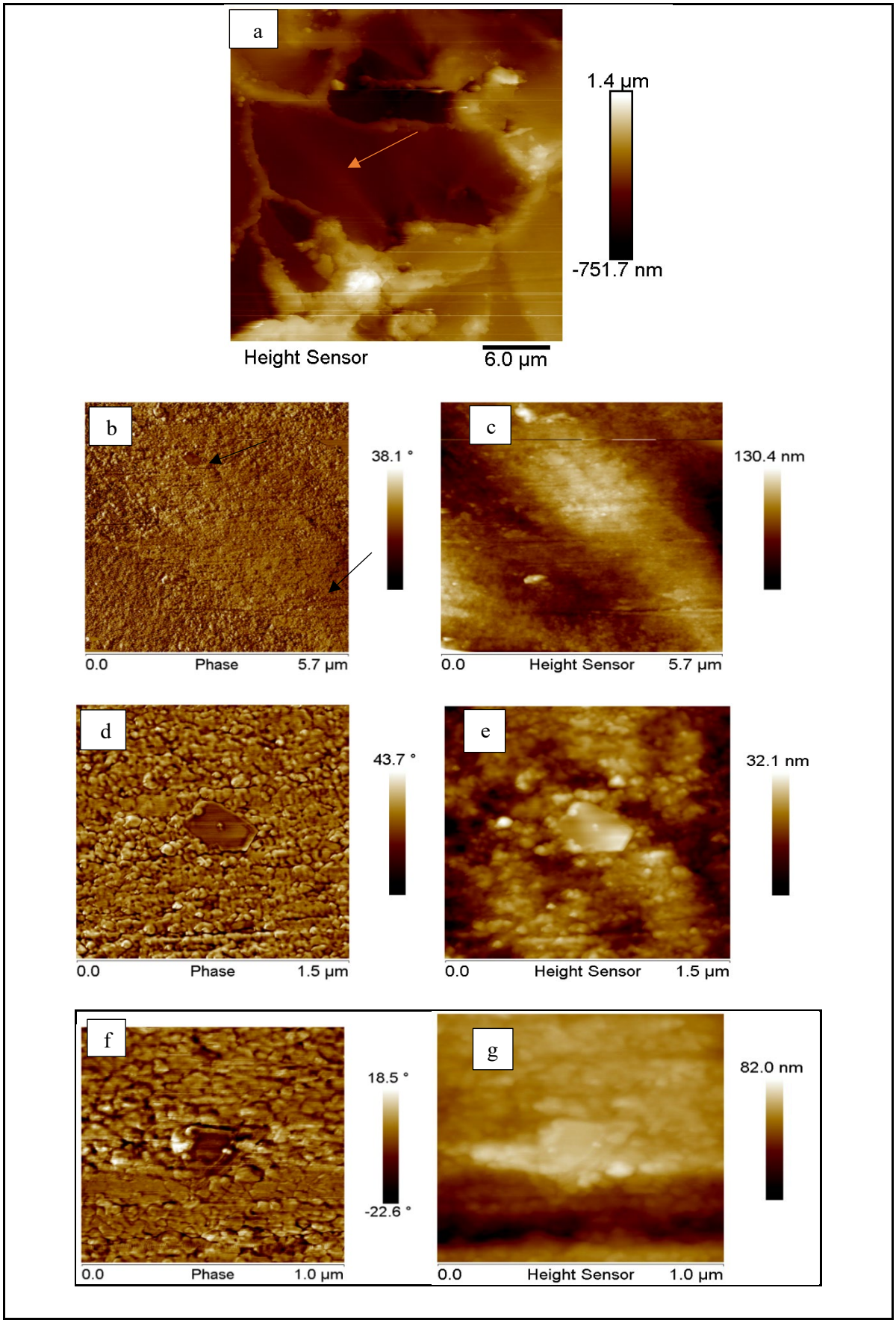

Figure 6. (a-g): Tapping mode QNM images for a specific area in a cryogenic fracture surface.

Images –d- and –e- in Figure 6 show the height sensor channel and the phase channel; respectively, for the upper left GO flake that appear in images b and c. Images –f- and –g- show the height sensor channel and the phase channel; respectively, for the lower right GO flake.

The scale bars related to images –a-, -b-, -d- and –f- of Figure 6 represent the Z-axis which shows the distance ramped by the piezo scanner in the vertical direction [45].

After producing the tapping mode imaging, the peak force QNM was used for nanomechanical characterization purposes. This was carried out for both the two detected GO flakes on the cryogenic fracture surface and the polymer matrix of PS surrounding them. The DMT modulus maps were used to achieve this goal.

Figure 7 includes images of DMT modulus maps for GO flakes and the PS matrix around them. Table 2 shows the modulus and standard deviation for the flakes and the matrix achieved by the nanomechanical characterization using peak force QNM.

Image –a- in Figure 7 represents the height sensor channel of the lower right flake. The mean height of the flake with respect to the matrix above it is 6.5 nm. Image – b – shows the DMT modulus channel for the same flake. Image – c- shows the DMT modulus channel with a mask drawn over the flake (the red area) and this mask is drawn by using a software tool described in the experimental section. The mean and standard deviation of the pixel values within and outside the mask allow the modulus of the flake and the matrix to be estimated.

Image (d) in Figure 7 shows the height channel sensor for the upper left flake of GO. The mean height of the flake with respect to the matrix is 9.5 nm.

Images (e and f) show the modulus channel and the mask over the channel for the upper left flake respectively. The mask is drawn over the flake, and in the DMT modulus channel and the mean of the pixel values is calculated inside and outside the mask.

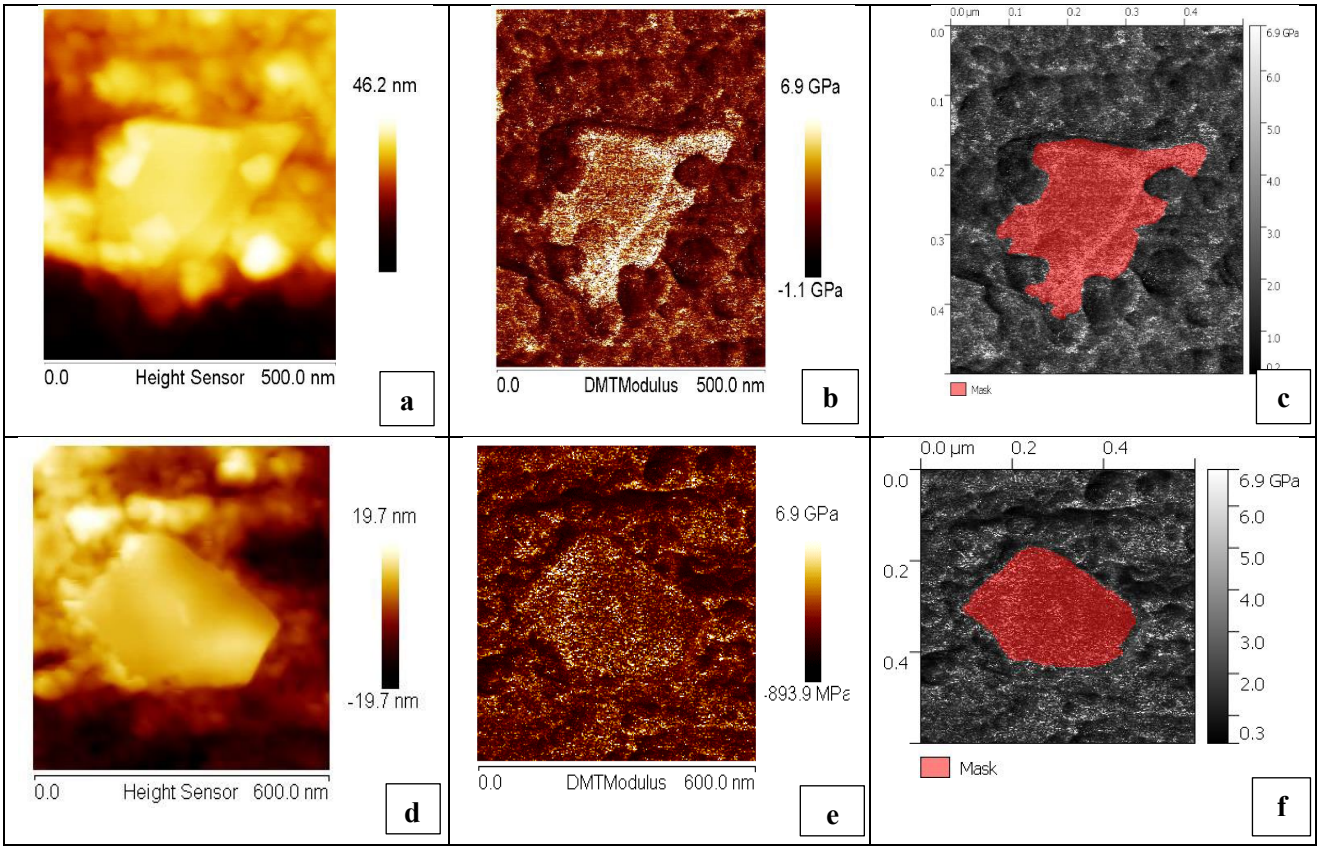

Figure 7 (a-f): Height sensor channels, DMT modulus channels and the red mask for DMT modulus channels for both the lower right GO flake (a-c images) and upper left GO flake (d-f images).

Table 2: Quantitative nano-mechanical measurements for GO flakes and PS.

Sample	**DMT Modulus / GPa**
GO flake " Lower right"	3.7 $\pm$ 1.9
PS matrix around lower right flake	1.9 $\pm$ 1.1
GO flake " Upper Left"	2.4 $\pm$ 1.3
PS matrix around upper left flake	1.7 $\pm$ 1.0

The measured Young's modulus of the PS matrix is within the expected range. However, while the Young's modulus of the GO flakes is significantly higher than the PS matrix, this difference is significantly lower than expected.

Possible explanations for this is that the flakes have some residual PS on their upper surface and the tip may have become contaminated with PS from the matrix. Hence, the measured features are not actually GO, but rather some other contaminants on the sample surface, or that the features are GO flakes that have been pulled free from the opposing half of the fracture surface and are only partially embedded in the imaged surface, with the free, measured part of the flake being stuck down to the surface of the PS matrix by capillary and Van der Waals forces. This would lead to the measured mechanical properties reflecting a combination of the forces immobilizing free part the flake and the flake itself.

The polymer chain orientation and the crystallinity of the polymer at the nano-scale play an important role in measuring Young's modulus for polymers. The standard deviation is obtained for GO and PS as this technique can provide repeatable measurements of Young's modulus at the nano-scale using a range of probes with taking in consideration the inevitability of providing the required calibration. The lower standard deviation for the above results shown in table 2 indicates a high precision of measurements. The considerable difference between the results obtained by the conventional AFM and peak force QNM can be ascribed to the difference in the stiffness of the used cantilevers. Regarding the experimental section, the radius of the tip used is very fine (less than 25 nm) and this is a requirement for obtaining better imaging resolution with optimum indentations at the nano- scale [46].

Generally Young's modulus at the nano-scale for polymers is measured by depositing the polymer film with a specific thickness over the silicon substrate. In this study, the modulus is taken by indenting the tip on the cryogenic fracture surface directly.

The Deposition of several polymers, including PS, over a silicon substrate has been reported and they used a specific probe to find the modulus for these polymers at the nano-scale. The obtained modulus using this approach is expected to be overestimated as the deformation of the sample exceeded 10% of the thickness of the film [16]. Several authors [20] studied the nanomechanical properties for the polymer surface for several polymers including PS. This approach requires a careful selection of the tips and cantilevers in order to obtain the right modulus. Use of a range of tips starting from Berkovich indenter of nanoindentation and three other different cantilevers manufactured from different materials with high spring constants ranging from 56 Nm^{-1} to 227 Nm^{-1} has also been reported and the results showed a slightly higher modulus for PS (3.24 GPa) compared with the modulus provided by the supplier of (3.0 GPa) and the standard deviation in the four cases was low. The values of Young's modulus for the polymer in the current study are quite reasonable. Despite the fact that co-authors used the JKR model for finding Young's modulus for PS [17], they used a tip that has a spring constant quite similar to the one used in the current study. The result refers to 2.6 GPa at a deformation of about 1.7 nm which is slightly higher than the one obtained in this study [20]. The moduli for GO flakes appear to be underestimated. Some researchers reported the value of Young modulus for a single layer graphene sheet at 1100 GPa [6]. The Molecular Dynamics MD simulation was used to calculate Young's modulus for GO and it was found that the value of the modulus varies from (290-430) GPa for amorphous GO and from (380-470) GPa for ordered GO depending on the coverage of the functional groups [47].

Furthermore, the mechanical properties of free standing GO by using nanoindentation combined with the dynamic contact module DCM has been reported [48]. The deposited GO film of thickness ~50-60 nm had a Young's modulus of (695 + 53 ~ 697 + 15) GPa which is higher than the modulus of a single layer of graphene sheet (0.25 TPa). The high value of Young's modulus is related to the number of GO layers. In the aforementioned study [48], the crack propagation of (50-60) nm thickness of GO free standing film started to appear at loads of 65 and 72 μN. The tip used was a Berkovich indenter of nanoindentation. In the current study, the applied load was 10 nN only for the flakes that have a thickness of few nano-meters. The cantilever used in the current measurements is unlikely to be stiff enough to provide sufficient indentation on the GO flake. In the event of further force applied over the tip, then the tip geometry will be changed resulting in blurry images. Furthermore, there are other limitations for peak force QNM that can adversely affect the results (for both the polymer and the flakes). One important example is the complex force interaction between the tips and different surfaces that arises from tip - surface contact. This leads to inaccurate measurements. As described in the introduction, the most used mathematical relations for finding the Young's modulus at the nano-scale for polymers and nanoparticles are Hertzian, DMT and JKR. These are estimated on the basis of the contact between the spherical tip of specific radius and a flat surface of the sample. Moreover, ''the tip apex may differ from an ideal sphere'' which can lead to major errors in calculations of the modulus. The AFM tip is also prone to lateral and buckling movement (as rotation) and this is another reason for the unexpected results for nanomechanical measurements.

S-SNOM

Tip-surface shear forces are generated as a result of this rotational movement during the cantilever deflection and they are not accounted for in the aforementioned mathematical models [20]. Figure 8 shows the cryogenically fractured service of PS/GO by tip-force mode related to s-SNOM.

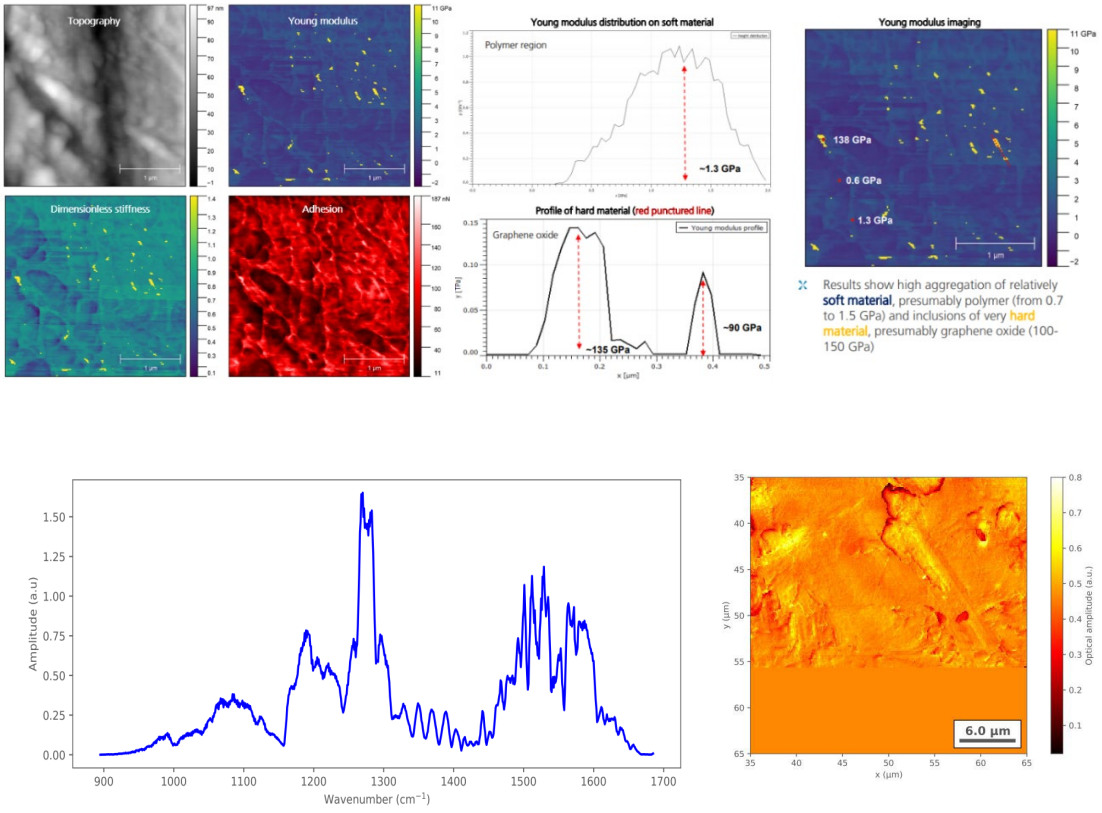

Figure 8: The nanomechanical findings with Nano IR spectra for the cryogenically fractured surface of PS/GO 1.0 wt. % nanocomposite obtained by s-SNOM.

IR s-SNOM imaging and Nano FTIR are novel techniques that provide fast and detailed nano-scale identification for different polymeric constituents, blends, and composites throughout an efficient combination of high resolution spectroscopy and microscopy. This means that a very short period of time would be needed to investigate the distribution of the components and their phase boundaries within resolutions down to 20 nm. It was confirmed that PS is among the widely distributed polymers which was difficult to be identified by near field spectroscopy.

The optical contrasts and clear phase differentiation are obvious in the image located next to nano-FTIR peaks of PS. These contrasts are reflecting the differences in energy dissipation between the tip and the sample [49]. 1445, 1486, and 1600 cm^{-1} of CH_2 bend, aromatic ring stretch, and benzene ring stretch; respectively are the main peaks of PS that can be seen in nano FTIR data which are stand next to AFM image of Figure 8. The factors that influencing the obtained data are: Interaction between the tip and the sample, infinitesimal alterations in the surface, and environmental circumstances [49]. Results obtained by s-SNOM are in line with the other microscopic findings reported in this work. The GO nano-sheets are dispersed homogeneously within the polymeric medium of PS, as shown by Young's modulus imaging in Figure 8, which is confirmed by OM, SEM, and TEM. The Young's modulus for PS obtained by Tip-Force is varied between (0.7 – 1.3) GPa depending on the position of indentation. As shown by the nanomechanical measurements in Figure 8, the highest Young's modulus for PS is achieved in regions close to the GO nano-sheets (yellow particles), whereas the lowest value of Young's modulus for PS achieved where the cantilever is indented in a region far away from the nano-sheets. This outcome can pave the way towards a promising study related to the interphase in polymer nanocomposites as this parameter still represents a challenging factor in the world of composites. The findings achieved by Tip-Force and QNM can be linked together as the values of Young's modulus for PS are quite similar especially those values achieved where the cantilever indented close to GO nano-sheets. The employment of a dull probe with an indentation depth varied between (2-10) nm showed a Young's modulus of (1.6$\pm$ 0.4) GPa for PS which is quite close to the obtained values in this section. On the other hand, an overestimation of Young's modulus reached up to (3.7$\pm$ 0.6) GPa when a sharp probe with a range of indentation

depth varied from (1-3) nm. The reasons behind this overestimation was intimately associated with the viscoelastic response of the sample, sample aging near the surface, and sample creep [50]. In addition, the Young's modulus for GO nano-sheets recorded 130 GPa using Tip-Force.

Conclusion

Evaluation of the nanomechanical behaviour of polymer nanocomposites is essential. The depth of indentation, the nature of the cantilever, the sensitivity of the machine, play a vital role in in understanding the nanomechanical behaviour of polymer nanocomposites. Surface properties of the nanocomposites are also crucial for their mechanical behaviour. In this study cryogenically fractured surface was used to obtain Young's modulus in nano-scale for the polymer and for the nano-material as findings could not be reached for the bulk surface due to low weight fraction of the nano-material incorporated in the polymer. It was a challenging task and a novel approach that did not witness a growing body in the literature. Microscopic techniques, such as s-SNOM, employed in this study, allowed to understand the nanomechanical behaviour of PS/GO nanocomposite.

Acknowledgements

The first author would like to thank his employer; The Ministry of Higher Education and Scientific Research MOHESR as well as his academic institution; University of Technology- Iraq for the financial and moral support. He would also like to thank Jamie Hobbs, The Department of Physics at The University of Sheffield, UK for facilitating the access to the Dimension Icon AFM used for the PeakForce QNM measurements. Sincere thankfulness and appreciation to Attocube Systems, Munich, Germany for the diligent and dedicated effort in carrying out the required measurements S-SNOM. Special thanks and sincere appreciation to Prof. Mohammed Sapuan Salit from Faculty of Engineering, Universiti Putra Malaysia UPM for his kind and professional role that help to accomplish this work.

Conflicts of Interest: The authors declare no conflict of interest.

References

[1] K.V. Maheshkumar, K. Krishnamurthy, P. Sathishkumar, S. Sahoo, E. Uddin, S.K. Pal, R. Rajasekar, (2014, January). "Research updates on Graphene oxide based polymeric nanocomposites". *Polymer composites*. Vol. 35, No. 12, pp.1–14. https://doi.org/10.1002/pc.22899.

[2] K. Singh, A. Ohlan, A. & S.K. Dhawan. "Polymer-Graphene Nanocomposites: Preparation, Characterization, Properties, and Applications", in *Nanocomposites- New trends and developments*, F. Ebrahimi, London: Intech Open, 2012, pp. 1-36. http://dx.doi.org/10.5772/50408.

[3] Z.B. Abd, N.A. Habib, A. Khammas, (2022, June). "A Physico-Chemical Contribution to the Conventional Technique of Preparation Graphene Oxide", *Journal of Applied Sciences and Nanotechnology*, Vol. 2, No. 2, pp. 70-78. DOI: 10.53293/jasn.2021.4296.1090.

[4] S. Guo & S. Dong, (2011, January). "Graphene nano-sheet: synthesis, molecular engineering, thin film, hybrids, and energy and analytical applications". *Chemical Society reviews*, Vol. 40, No. 5, pp.2644–2672. https://doi.org/10.1039/C0CS00079E.

[5] X. Huang, X. Qi, F. Boey & H. Zhang, (2012, January). "Graphene-based composites". *Chemical Society Reviews*, Vol. 41, No. 2, pp.666–686. https://doi.org/10.1039/C1CS15078B.

[6] X. Sun, H. Sun, H. Li, & H. Peng, (2013, October). "Developing polymer composite materials: Carbon nanotubes or graphene?". *Advanced Materials*, Vol. 25, No. 37, pp.5153–5176. https://doi.org/10.1002/adma.201301926.

[7] K. H. Liao, A. Mittal, S. Bose, C. Leighton, K. A. Mkhoyan, & C. W. Macosko, (2011, January). "Aqueous Only Route toward Graphene from Graphite Oxide". *ACS Nano*. Vol. 5, No. 2, pp: 1253-1258. https://doi.org/10.1021/nn1028967.

[8] K. A. Mkhoyan, A. W. Contryman, J. Silcox, D. A. Stewart, G. Eda, C. Mattevi, S. Miller, & M. Chhowalla, (2009, February). "Atomic and Electronic Structure of Graphene-Oxide". *Nano Letters*, Vol. 9, No. 3, pp.1058–1063. https://doi.org/10.1021/nl8034256.

[9] R. Gu, W. Z. Xu, P. A. Charpentier, (2014, September). "Synthesis of graphene-polystyrene nanocomposites via RAFT polymerization". *Polymer*, Vol. 55, No. 21, pp. 5322-5331. http://dx.doi.org/10.1016/j.polymer.2014.08.064.

[10] H. J. Salavagione, G. Martinez & G. Ellis. "Graphene-based polymer nanocomposites", in *Physics and applications of graphene*, Dr. S. Mikhailov, London: Intech Open, 2011, pp. 1–14. http://www.intechopen.com/books/physics-and-applications-of-grapheneexperiments/graphene-based-polymer-nanocomposites.

[11] F. Hussain, M. Hojjati, M. Okamoto, R.E. Gorga, (2006, March). "Review article: Polymer-matrix Nanocomposites, Processing, Manufacturing, and Application: An Overview". *Journal of Composite Materials.* Vol. 40, No. 17, pp. 1511-1577. https://doi.org/10.1177/0021998306067321.

[12] Y. Zhu, D. Gianola, & T. Zhu, (2016, July). "Editorial for the focus issue on Nanomechanics in Extreme Mechanics Letters". *Extreme Mechanics Letters*, Vol. 8, pp.125–126. http://dx.doi.org/10.1016/j.eml.2016.07.008.

[13] H.J. Butt, B. Cappella, M. Kappl, (2005, October). "Force measurements with the atomic force microscope: Technique, interpretation and applications". *Surface Science Reports*, Vol. 59, No. 1-6, pp.1–152. https://doi.org/10.1016/j.surfrep.2005.08.003

[14] B. Cappella, G. Dietler, (1999, November), "Force-distance curves by atomic force microscopy". *Surface Science Reports,* Vol. 34, No. (1-3); pp. 5-104. https://doi.org/10.1016/S0167-5729(99)00003-5.

[15] D. Bonnell, (2001, January). *Scanning probe microscopy and spectroscopy: Theory, techniques, and applications* (2nd Edition), Canada: John Wiley and Sons. [Online]. Available: https://www.wiley.com/en-ie/Scanning+Probe+Microscopy+and+Spectroscopy:+Theory,+Techniques,+and+Applications,+2nd+Edition-p-9780471248248.

[16] G. Smolyakov, S. Pruvost, L. Cardoso, B. Alonso, E. Belamie, J. D. Rumeau, (2016, May). "AFM PeakForce QNM mode: Evidencing nano-meter scale mechanical properties of chitin-silica hybrid nanocomposites". *Carbohydrate Polymers*, Vol. 151, pp.373–380. http://dx.doi.org/10.1016/j.carbpol.2016.05.042.

[17] L.Y. Lin, & D.E. Kim, (2012, October). "Measurement of the elastic modulus of polymeric films using an AFM with a steel micro-spherical probe tip". *Polymer Testing*, Vol.31, No.7, pp. 926-930. http://dx.doi.org/10.1016/j.polymertesting.2012.06.012 .

[18] C.A. Clifford & M.P. Seah, (2005, July). "The determination of atomic force microscope cantilever spring constants via dimensional methods for nanomechanical analysis". *Nanotechnology*, Vol. 16, No. 9, pp.1666–1680. Online at: stacks.iop.org/Nano/16/1666. **DOI** 10.1088/0957-4484/16/9/044.

[19] D. M. Panaitescu, Z. Vuluga, C. Radovici, C. Nicolae, (2012, April). "Morphological investigation of PP/nano-silica composites containing SEBS". *Polymer Testing*, Vol. 31, No. 2, pp.355–365. https://doi.org/10.1016/j.polymertesting.2011.12.010.

[20] T. J. Young, M. A. Monclus, T. L. Burnett, W. R. Broughton, S. L. Ogin, & P. A. Smith, (2011, October). "The use of the PeakForce quantitative nanomechanical mapping AFM-based method for high-resolution Young's modulus measurement of polymers". *Measurement Science and Technology*, Vol. 22, No. 12, pp.1–6. https://doi.org/10.1088/0957-0233/22/12/125703 .

[21] M. Goikoetxea, I. Amenabar, S. Chimenti, M. Paulis, J. R. Leiza, & R. Hillenbrand, (2021, January). "Cross-Sectional Chemical Nano-imaging of Composite Polymer Nanoparticles by Infrared Nano-spectroscopy". *Macromolecules*, Vol. 54, No. 2, pp. 995−1005. https://dx.doi.org/10.1021/acs.macromol.0c02287.

[22] A. Walter, J.G. Mannheim, C.J. Caruana, (2021, May). *Imaging Modalities for Biological and Preclinical Research: A Compendium* (Volume 1). [Online]. IOP Publishing, Bristol, UK. http://iopscience.iop.org/book/978-0-7503-3059-6 .

[23] D. Vobornik, G. Margaritondo, J.S. Sanghera, P. Thielen, I.D. Aggarwal, B. Ivanovc, N.H. Tolk, V. Mannid, S. Grimaldi, A. Lisi, S. Rieti, D.W. Piston,

R. Generosi, M. Luce, P. Perfetti, A. Cricenti, (2005, September). "Spectroscopic infrared scanning near-field optical microscopy (IR-SNOM)". *Journal of Alloys and Compounds*, Vol. 401, No. 1-2, pp. 80–85. https://doi.org/10.1016/j.jallcom.2005.02.057.

[24] P. Bazylewski, S. Ezugwu & G. Fanchini, (2017, September). "A Review of Three-Dimensional Scanning Near-Field Optical Microscopy (3D-SNOM) and Its Applications in Nanoscale Light Management". *Appl. Sci*., Vol. 7, No. 10, 973, pp. 1-25. https://doi.org/10.3390/app7100973.

[25] Z.G. Mohammadsalih, B.J. Inkson, B. Chen, (2021, January). "The Effect of Dispersion Condition on the Structure and Properties of Polystyrene/Graphene Oxide Nanocomposites". *Polym. Compos*, Vol. 42, No.1, pp. 320–328. https://doi.org/10.1002/pc.25827.

[26] Z.G. Mohammadsalih & N.S. Sadeq, (2022, January). "Structure and properties of polystyrene/graphene oxide nanocomposites". *Fullerenes, Nanotubes, and Carbon Nanostructures,* Vol. 30, No. 3, pp. 373–384. https://doi.org/10.1080/1536383X.2021.1943367.

[27] D.C. Marcano, D.V. Kosynkin, J.M. Berlin, A. Sinitskii, Z. Sun,

A. Slesarev, L.B. Alemany, W. Lu, & J.M. Tour, (2010, July). "Improved Synthesis of Graphene Oxide". *ACS Nano*, Vol. 4, No. 8, pp.4806–4814. https://doi.org/10.1021/nn1006368.

[28] R. Ming, Y. Ding, F. Chang, X. He, J. Feng, C. Wang, P. Zhang, (2013, February). "Humidity-dependant compression properties of graphene oxide foams prepared by freeze-drying technique". *Micro & Nano Letters*, Vol. 8, No. 2, pp.66–67. https://doi.org/10.1049/mnl.2012.0833.

[29] S.I. Kattimuttathu, C. Krishnappan, V. Vellorathekkaepadil, R. Nutenkia, V.R. Mandapati, & M. Černík, (2015, March). "Synthesis, characterization and optical properties of graphene oxide polystyrene nanocomposites". *Polym.Adv.Technol*, Vol. 26, No. 3, pp.214–222. https://doi.org/10.1002/pat.3435.

[30] M. Bera, Chandravati, P. Gupta, and P.K. Maji, (2018, February). " Facile One-Pot Synthesis of Graphene Oxide by Sonication Assisted Mechanochemical Approach and Its Surface Chemistry". *Journal of Nanoscience and Nanotechnology*, Vol. 18, No. 2, pp. 902-912. Doi: 10.1166/jnn.2018.14306.

[31] S. Drewniak, R. Muzyka, A. Stolarczyk, Tadeusz Pustelny,

M.K. Moranska, & M. Setkiewicz, (2016, January). "Studies of Reduced Graphene Oxide and Graphite Oxide in the Aspect of Their Possible Application in Gas Sensors". *Sensors (Basel, Switzerland)*, Vol. 16, No. 1-103, pp. 1-16. https://doi.org/10.3390/s16010103.

[32] C. Xu, X. Shi, A. Ji, L. Shi, C. Zhou, Y. Cui , (2015, December). "Fabrication and characteristics of reduced graphene oxide produced with different green reductants". *PLoS ONE*, Vol. 10, No. 12, pp.1–15.

http://210.73.128.105/cpsb/CPSB/login.jsp?typ = nolog.

[33] S. Basu, M. Singhi, B.K. Satapathy, M. Fahim, (2013, December). "Dielectric, electrical and rheological characterization of graphene filled Polystyrene nanocomposites". *Polymer composite*, Vol. 34, No. 12, pp.2082–2093. https://doi.org/10.1002/pc.22617.

[34] S.K. Yadav & J.W. Cho, (2013, February). "Functionalized graphene nanoplatelets for enhanced mechanical and thermal properties of polyurethane nanocomposites". *Applied Surface Science*, Vol. 266, pp.360–367. http://dx.doi.org/10.1016/j.apsusc.2012.12.028 .

[35] C. Wan & B. Chen, (2012, January). "Reinforcement and interphase of polymer/graphene oxide nanocomposites". *Journal of Materials Chemistry*, Vol. 22, No. 8, pp.3637–3646. https://doi.org/10.1039/C2JM15062J.

[36] D.R. Paul & L.M. Robeson, (2008, July). "Polymer nanotechnology: Nanocomposites". *Polymer*, Vol. 49, No.15, pp.3187–3204. https://doi.org/10.1016/j.polymer.2008.04.017.

[37] S.G. Prolongo, M. Buron, M.R. Gude, R. Chaos-Moran, M. Campo, A. Urena, (2008, October). "Effects of dispersion techniques of carbon nanofibers on the thermo-physical properties of epoxy nanocomposites". *Composites Science and Technology*, Vol. 68, No. 13, pp.2722–2730. https://doi.org/10.1016/j.compscitech.2008.05.015.

[38] B.V. Derjaguin, V.M. Muller, & Y.P. Toporov, (1975, November). "Effect of contact deformation on the adhesion of particles". *Journal of colloid and interface science*, Vol. 53, No. 2, pp.314–326. https://doi.org/10.1016/0021-9797(75)90018-1.

[39] V.M. Muller, B.V. Derjaguin, & Y.P. Toporov, (1983, August). "On two methods of calculation of the force of sticking of an elastic sphere to a rigid plane". *Colloids and Surfaces*, Vol. 7, No. 3, pp.251–259. https://doi.org/10.1016/0166-6622(83)80051-1 .

[40] E.R. Beach, G.W. Tormoen, J. Drelich, & R. Han, (2002, March). "Pull-off force measurements between rough surfaces by atomic force microscopy". *Journal of colloid and interface science*, Vol. 247, No. 1, pp.84–99. https://doi.org/10.1006/jcis.2001.8126.

[41] B.J.R. Thio, & J.C. Meredith, (2007, October). "Measurement of polyamide and polystyrene adhesion with coated-tip atomic force microscopy". *Journal of Colloid and Interface Science*, 314(1), pp.52–62. https://doi.org/10.1016/j.jcis.2007.05.029.

[42] M. Xing, W. Zhong, X. Xu, & D. Thomson, (2010, June). "Adhesion force studies of nanofibers and nanoparticles". *Langmuir*, Vol. 26, No. 14, pp.11809–11814. https://doi.org/10.1021/la100443d.

[43] D.M. Panaitescu, A.N. Frone, Cristian Nicolae, (2013, October). "Micro- and nano-mechanical characterization of polyamide 11 and its composites containing cellulose nanofibers". *European Polymer Journal*, Vol. 49, No. 12, pp.3857–3866. http://dx.doi.org/10.1016/j.eurpolymj.2013.09.031 .

[44] R.M. Grigorescu, F. Ciuprina, P. Ghioca, M. Ghiurea, L. Iancu, B. Spurcaciu, D.M. Panaitescu, (2016, February). "Mechanical and dielectric properties of SEBS modified by graphite inclusion and composite interface". *Journal of Physics and Chemistry of Solids*, Vol. 89, pp.97–106. http://dx.doi.org/10.1016/j.jpcs.2015.10.008.

[45] D.E. Martinez-Tong, A.S. Najar, M. Soccio, A. Nogales, N. Bitinis, M.A. Lopez Manchado, T.A. Ezquerra, (2014, November). "Quantitative mapping of mechanical properties in polylactic acid/natural rubber/organoclay bio-nanocomposites as revealed by nanoindentation with atomic force microscopy". *Composites Science and Technology*, Vol. 104, pp.34–39. http://dx.doi.org/10.1016/j.compscitech.2014.08.030

[46] "Nanoindentation and Nanoscratching with SPMs For NanoScope™ Version 5.30 Rev.2 Software", Veeco, Santa Barbara, Canada, Support Note No. 013-225-000, 2005.

[47] L. Liu, J. Zhang, J. Zhao, & F. Liu, (2012, July). "Mechanical properties of graphene oxides". *Nanoscale*, Vol. 4, No. 19, pp.5910–5916. https://doi.org/10.1039/C2NR31164J .

[48] S.H. Kang, T.H. Fang, Z.H. Hong, C.H. Chuang, (2013, September). "Mechanical properties of free-standing graphene oxide". *Diamond and Related Materials*, Vol. 38, pp.73–78. http://dx.doi.org/10.1016/j.diamond.2013.06.016 .

[49] M. Meyns, S. Primpke, G. Gerdts, (2019, September). Library based identification and characterisation of polymers with nano-FTIR and IR-sSNOM imaging. *Journal of Analytical Methods*, Vol. 11, No. 40, pp: 1-23. https://doi.org/10.1039/C9AY01193E .

[50] M. Dokukin & I. Sokolov, (2012, October). Quantitative Mapping of the Elastic Modulus of Soft Materials with HarmoniX and PeakForce QNM AFM Modes. Langmuir, Vol. 28, No. 46, pp. 16060−16071. https://doi.org/10.1021/la302706b.